High-resolution image reconstruction with latent diffusion models from human brain activity

Yu Takagi[1,2*]   Shinji Nishimoto[1,2]

[1]Graduate School of Frontier Biosciences, Osaka University, Japan

[2]CiNet, NICT, Japan

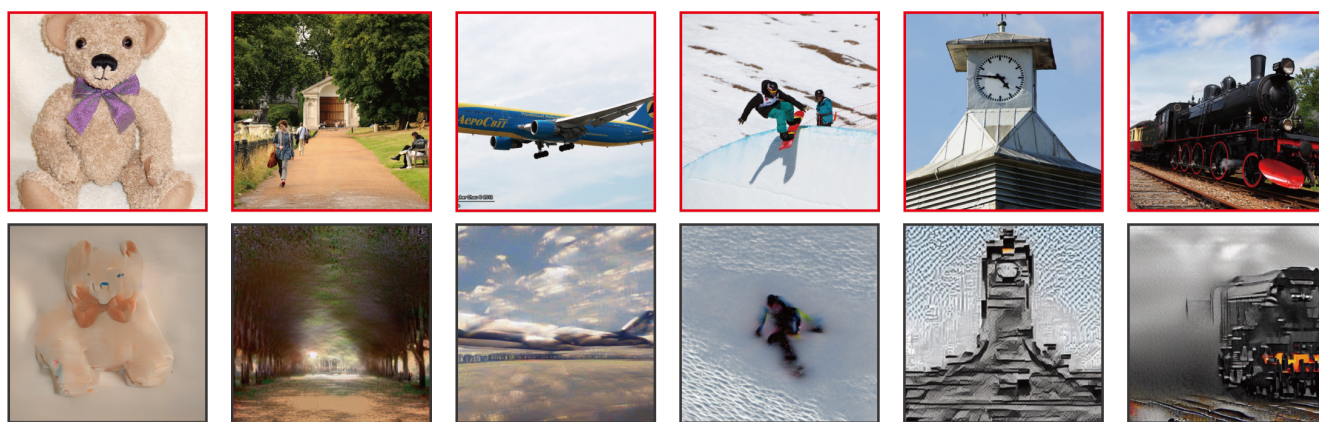{takagi.yuu.fbs,nishimoto.shinji.fbs}@osaka-u.ac.jp

Figure 1. Presented images (red box, top row) and images reconstructed from fMRI signals (gray box, bottom row) for one subject (subj01).

Abstract

Reconstructing visual experiences from human brain activity offers a unique way to understand how the brain represents the world, and to interpret the connection between computer vision models and our visual system. While deep generative models have recently been employed for this task, reconstructing realistic images with high semantic fidelity is still a challenging problem. Here, we propose a new method based on a diffusion model (DM) to reconstruct images from human brain activity obtained via functional magnetic resonance imaging (fMRI). More specifically, we rely on a latent diffusion model (LDM) termed Stable Diffusion. This model reduces the computational cost of DMs, while preserving their high generative performance. We also characterize the inner mechanisms of the LDM by studying how its different components (such as the latent vector of image Z, conditioning inputs C, and different elements of the denoising U-Net) relate to distinct brain functions. We show that our proposed method can reconstruct high-resolution images with high fidelity in straight-forward fashion, without the need for any additional training and fine-tuning of complex deep-learning models. We also provide a quantitative interpretation of different LDM components from a neuroscientific perspective. Overall, our study proposes a promising method for reconstructing images from human brain activity, and provides a new framework for understanding DMs. Please check out our webpage at https://sites.google.com/view/stablediffusion-with-brain/.

1. Introduction

A fundamental goal of computer vision is to construct artificial systems that see and recognize the world as human visual systems do. Recent developments in the measurement of population brain activity, combined with advances in the implementation and design of deep neural network models, have allowed direct comparisons between latent representations in biological brains and architectural characteristics of artificial networks, providing important insights into how these systems operate [3, 8–10, 13, 18, 19, 21, 42, 43, 54, 55]. These efforts have in-

---

* Corresponding author

cluded the reconstruction of visual experiences (perception or imagery) from brain activity, and the examination of potential correspondences between the computational processes associated with biological and artificial systems [2, 5, 7, 24, 25, 27, 36, 44–46].

Reconstructing visual images from brain activity, such as that measured by functional Magnetic Resonance Imaging (fMRI), is an intriguing but challenging problem, because the underlying representations in the brain are largely unknown, and the sample size typically associated with brain data is relatively small [17, 26, 30, 32]. In recent years, researchers have started addressing this task using deep-learning models and algorithms, including generative adversarial networks (GANs) and self-supervised learning [2, 5, 7, 24, 25, 27, 36, 44–46]. Additionally, more recent studies have increased semantic fidelity by explicitly using the semantic content of images as auxiliary inputs for reconstruction [5, 25]. However, these studies require training new generative models with fMRI data from scratch, or fine-tuning toward the specific stimuli used in the fMRI experiment. These efforts have shown impressive but limited success in pixel-wise and semantic fidelity, partly because the number of samples in neuroscience is small, and partly because learning complex generative models poses numerous challenges.

Diffusion models (DMs) [11, 47, 48, 53] are deep generative models that have been gaining attention in recent years. DMs have achieved state-of-the-art performance in several tasks involving conditional image generation [4, 39, 49], image super resolution [40], image colorization [38], and other related tasks [6, 16, 33, 41]. In addition, recently proposed latent diffusion models (LDMs) [37] have further reduced computational costs by utilizing the latent space generated by their autoencoding component, enabling more efficient computations in the training and inference phases. Another advantage of LDMs is their ability to generate high-resolution images with high semantic fidelity. However, because LDMs have been introduced only recently, we still lack a satisfactory understanding of their internal mechanisms. Specifically, we still need to discover how they represent latent signals within each layer of DMs, how the latent representation changes throughout the denoising process, and how adding noise affects conditional image generation.

Here, we attempt to tackle the above challenges by reconstructing visual images from fMRI signals using an LDM named Stable Diffusion. This architecture is trained on a large dataset and carries high text-to-image generative performance. We show that our simple framework can reconstruct high-resolution images with high semantic fidelity without any training or fine-tuning of complex deep-learning models. We also provide biological interpretations of each component of the LDM, including forward/reverse

diffusion processes, U-Net, and latent representations with different noise levels.

Our contributions are as follows: (i) We demonstrate that our simple framework can reconstruct high-resolution (512×512) images from brain activity with high semantic fidelity, without the need for training or fine-tuning of complex deep generative models (Figure 1); (ii) We quantitatively interpret each component of an LDM from a neuroscience perspective, by mapping specific components to distinct brain regions; (iii) We present an objective interpretation of how the text-to-image conversion process implemented by an LDM incorporates the semantic information expressed by the conditional text, while at the same time maintaining the appearance of the original image.

2. Related Work

2.1. Reconstructing visual image from fMRI

Decoding visual experiences from fMRI activity has been studied in various modalities. Examples include explicitly presented visual stimuli [17, 26, 30, 32], semantic content of the presented stimuli [15, 31, 52], imagined content [13, 29], perceived emotions [12, 20, 51], and many other related applications [14, 28]. In general, these decoding tasks are made difficult by the low signal-to-noise ratio and the relatively small sample size associated with fMRI data.

While early attempts have used handcrafted features to reconstruct visual images from fMRI [17, 26, 30, 32], recent studies have begun to use deep generative models trained on a large number of naturalistic images [2, 5, 7, 24, 25, 27, 36, 44–46]. Additionally, a few studies have used semantic information associated with the images, including categorical or text information, to increase the semantic fidelity of the reconstructed images [5, 25]. To produce high-resolution reconstructions, these studies require training and possibly fine-tuning of generative models, such as GANs, with the same dataset used in the fMRI experiments. These requirements impose serious limitations, because training complex generative models is in general challenging, and the number of samples in neuroscience is relatively small. Thus, even modern implementations struggle to produce images, at most 256×256 resolution, with high semantic fidelity unless they are augmented with numerous tools and techniques. DMs and LDMs are recent algorithms for image generation that could potentially address these limitations, thanks to their ability to generate diverse high-resolution images with high semantic fidelity of text-conditioning, and high computational efficiency. However, to the best of our knowledge, no prior studies have used DMs for visual reconstruction.

2.2. Encoding Models

To understand deep-learning models from a biological perspective, neuroscientists have employed encoding models: a predictive model of brain activity is built out of features extracted from different components of the deep-learning models, followed by examination of the potential link between model representations and corresponding brain processes [3, 8–10, 13, 18, 19, 21, 42, 43, 54, 55]. Because brains and deep-learning models share similar goals (e.g., recognition of the world) and thus could implement similar functions, the ability to establish connections between these two structures provides us with biological interpretations of the architecture underlying deep-learning models, otherwise viewed as black boxes. For example, the activation patterns observed within early and late layers of a CNN correspond to the neural activity patterns measured from early and late layers of visual cortex, suggesting the existence of a hierarchical correspondence between latent representations of a CNN and those present in the brain [9, 10, 13, 19, 54, 55]. This approach has been applied primarily to vision science, but it has recently been extended to other sensory modalities and higher functions [3, 8, 18, 21, 42, 43].

Compared with biologically inspired architectures such as CNNs, the correspondence between DMs and the brain is less obvious. By examining the relationship between each component and process of DMs and corresponding brain activities, we were able to obtain biological interpretations of DMs, for example in terms of how latent vectors, denoising processes, conditioning operations, and U-net components may correspond to our visual streams. To our knowledge, no prior study has investigated the relationship between DMs and the brain.

Together, our overarching goal is to use DMs for high resolution visual reconstruction and to use brain encoding framework to better understand the underlying mechanisms of DMs and its correspondence to the brain.

3. Methods

Figure 2 presents an overview of our methods.

3.1. Dataset

We used the Natural Scenes Dataset (NSD) for this project [1]. Please visit the NSD website for more details [1]. Briefly, NSD provides data acquired from a 7-Tesla fMRI scanner over 30–40 sessions during which each subject viewed three repetitions of 10,000 images. We analyzed data for four of the eight subjects who completed all imaging sessions (subj01, subj02, subj05, and subj07). The images used in the NSD experiments were retrieved from MS COCO and cropped to 425×425 (if needed). We used
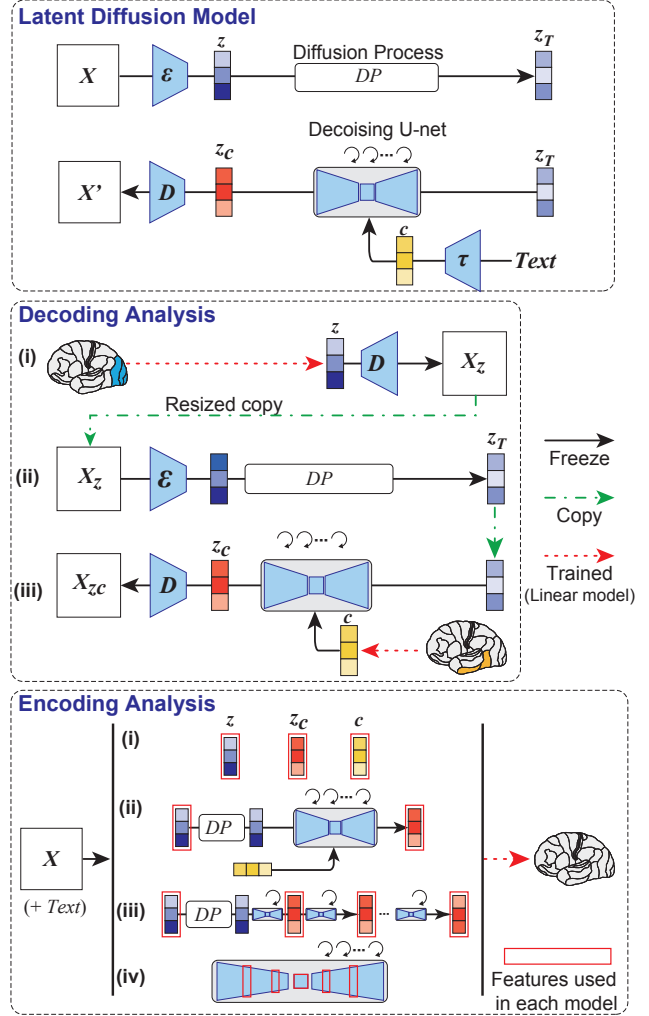
Figure 2. Overview of our methods. (Top) Schematic of LDM used in this study. ϵ denotes an image encoder, D is a image decoder, and τ is a text encoder (CLIP). (Middle) Schematic of decoding analysis. We decoded latent representations of the presented image ($\mathbf{z}$) and associated text $\mathbf{c}$ from fMRI signals within early (blue) and higher (yellow) visual cortices, respectively. These latent representations were used as input to produce a reconstructed image $\mathbf{X_{zc}}$. (Bottom) Schematic of encoding analysis. We built encoding models to predict fMRI signals from different components of LDM, including $\mathbf{z}$, $\mathbf{c}$, and $\mathbf{z_c}$.

27,750 trials from NSD for each subject (2,250 trials out of the total 30,000 trials were not publicly released by NSD). For a subset of those trials (N=2,770 trials), 982 images were viewed by all four subjects. Those trials were used as the test dataset, while the remaining trials (N=24,980) were used as the training dataset.

For functional data, we used the preprocessed scans (resolution of 1.8 mm) provided by NSD. See Appendix A for details of the preprocessing protocol. We used single-trial

beta weights estimated from generalized linear models and region of interests (ROIs) for early and higher (ventral) visual regions provided by NSD. For the test dataset, we used the average of the three trials associated with each image. For the training dataset, we used the three separate trials without averaging.

3.2. Latent Diffusion Models

DMs are probabilistic generative models that restore a sampled variable from Gaussian noise to a sample of the learned data distribution via iterative denoising. Given training data, the diffusion process destroys the structure of the data by gradually adding Gaussian noise. The sample at each time point is defined as $\mathbf{x}_t = \sqrt{\alpha_t}\mathbf{x}_0 + \sqrt{1 - \alpha_t}\epsilon_t$ where $\mathbf{x}_t$ is a noisy version of input $\mathbf{x}_0$, $t \in \{1, ..., T\}$, α is a hyperparameter, and ϵ is the Gaussian. The inverse diffusion process is modeled by applying a neural network $f_\theta(\mathbf{x}_t, t)$ to the samples at each step to recover the original input. The learning objective is $f_\theta(\mathbf{x}, t) \approx \epsilon_t$ [11, 47]. U-Net is commonly used for neural networks f_θ.

This method can be generalized to learning conditional distributions by inserting auxiliary input $\mathbf{c}$ into the neural network. If we set the latent representation of the text sequence to $\mathbf{c}$, it can implement text-to-image models. Recent studies have shown that, by using large language and image models, DMs can create realistic, high-resolution images from text inputs. Furthermore, when we start from source image with input texts, we can generate new text conditional images by editing the image. In this image-to-image translation, the degree of degradation from the original image is controlled by a parameter that can be adjusted to preserve either the semantic content or the appearance of the original image.

DMs that operate in pixel space are computationally expensive. LDMs overcome this limitation by compressing the input using an autoencoder (Figure 2, top). Specifically, the autoencoder is first trained with image data, and the diffusion model is trained to generate its latent representation $\mathbf{z}$ using a U-Net architecture. In doing so, it refers to conditional inputs via cross-attention. This allows for lightweight inference compared with pixel-based DMs, and for very high-quality text-to-image and image-to-image implementations.

In this study, we used an LDM called Stable Diffusion, which was built on LDMs and trained on a very large dataset. The model can generate and modify images based on text input. Text input is projected to a fixed latent representation by a pretrained text encoder (CLIP) [34]. We used version 1.4 of the model. See Appendix A for details on the training protocol.

We define $\mathbf{z}$ as the latent representation of the original image compressed by the autoencoder, $\mathbf{c}$ as the latent representation of texts (average of five text annotations asso-

ciated to each MS COCO image), and $\mathbf{z_c}$ as the generated latent representation of $\mathbf{z}$ modified by the model with $\mathbf{c}$. We used these representations in the decoding/encoding models described below.

3.3. Decoding: reconstructing images from fMRI

We performed visual reconstruction from fMRI signals using LDM in three simple steps as follows (Figure 2, middle). The only training required in our method is to construct linear models that map fMRI signals to each LDM component, and no training or fine-tuning of deep-learning models is needed. We used the default parameters of image-to-image and text-to-image codes provided by the authors of LDM [2], including the parameters used for the DDIM sampler. See Appendix A for details.

(i) First, we predicted a latent representation $\mathbf{z}$ of the presented image $\mathbf{X}$ from fMRI signals within early visual cortex. $\mathbf{z}$ was then processed by an decoder of autoencoder to produce a coarse decoded image $\mathbf{X_z}$ with a size of 320×320, and then resized it to 512×512.

(ii) $\mathbf{X_z}$ was then processed by encoder of autoencoder, then added noise through the diffusion process.

(iii) We decoded latent text representations $\mathbf{c}$ from fMRI signals within higher (ventral) visual cortex. Noise-added latent representations $\mathbf{z_T}$ of the coarse image and decoded $\mathbf{c}$ were used as input to the denoising U-Net to produce $\mathbf{z_c}$. Finally, $\mathbf{z_c}$ was used as input to the decoding module of the autoencoder to produce a final reconstructed image $\mathbf{X_{zc}}$ with a size of 512×512.

To construct models from fMRI to the components of LDM, we used L2-regularized linear regression, and all models were built on a per subject basis. Weights were estimated from training data, and regularization parameters were explored during the training using 5-fold cross-validation. We resized original images from 425×425 to 320×320 but confirmed that resizing them to a larger size (448×448) does not affect the quality of reconstruction.

As control analyses, we also generated images using only $\mathbf{z}$ or $\mathbf{c}$. To generate these control images, we simply omitted $\mathbf{c}$ or $\mathbf{z}$ from step (iii) above, respectively.

The accuracy of image reconstruction was evaluated objectively (perceptual similarity metrics, psms) and subjectively (human raters, N=6) by assessing whether the original test images (N=982 images) could be identified from the generated images. As a similarity metrics of PSMs, we used early/middle/late layers of CLIP and CNN (AlexNet) [22]. Briefly, we conducted two-way identification experiments: examined whether the image reconstructed from fMRI was more similar to the corresponding original image than randomly picked reconstructed image. See Appendix B for details and additional results.

---

[2]https://github.com/CompVis/stable-diffusion/blob/main/scripts/

3.4. Encoding: Whole-brain Voxel-wise Modeling

Next, we tried to interpret the internal operations of LDMs by mapping them to brain activity. For this purpose, we constructed whole-brain voxel-wise encoding models for the following four settings (see Figure 2 bottom and Appendix A for implementation details):

(i) We first built linear models to predict voxel activity from the following three latent representations of the LDM independently: $\mathbf{z}$, $\mathbf{c}$, and $\mathbf{z_c}$.

(ii) Although $\mathbf{z_c}$ and $\mathbf{z}$ produce different images, they result in similar prediction maps on the cortex (see 4.2.1). Therefore, we incorporated them into a single model, and further examined how they differ by mapping the unique variance explained by each feature onto cortex [23]. To control the balance between the appearance of the original image and the semantic fidelity of the conditional text, we varied the level of noise added to $\mathbf{z}$. This analysis enabled quantitative interpretation of the image-to-image process.

(iii) While LDMs are characterized as an iterative denoising process, the internal dynamics of the denoising process are poorly understood. To gain some insight into this process, we examined how $\mathbf{z_c}$ changes through the denoising process. To do so, we extracted $\mathbf{z_c}$ from the early, middle, and late steps of the denoising. We then constructed combined models with $\mathbf{z}$ as in the above analysis (ii), and mapped their unique variance onto cortex.

(iv) Finally, to inspect the last black box associated with LDMs, we extracted features from different layers of U-Net. For different steps of the denoising, encoding models were constructed independently with different U-Net layers: two from the first stage, one from the bottleneck stage, and two from the second stage. We then identified the layer with highest accuracy for each voxel and for each step.

Model weights were estimated from training data using L2-regularized linear regression, and subsequently applied to test data (see Appendix A for details). For evaluation, we used Pearson's correlation coefficients between predicted and measured fMRI signals. We computed statistical significance (one-sided) by comparing the estimated correlations to the null distribution of correlations between two independent Gaussian random vectors of the same length (N=982). The statistical threshold was set at $P < 0.05$ and corrected for multiple comparisons using the FDR procedure. We show results from a single random seed, but we verified that different random seed produced nearly identical results (see Appendix C). We reduced all feature dimensions to 6,400 by applying principal component analysis, by estimating components within training data.
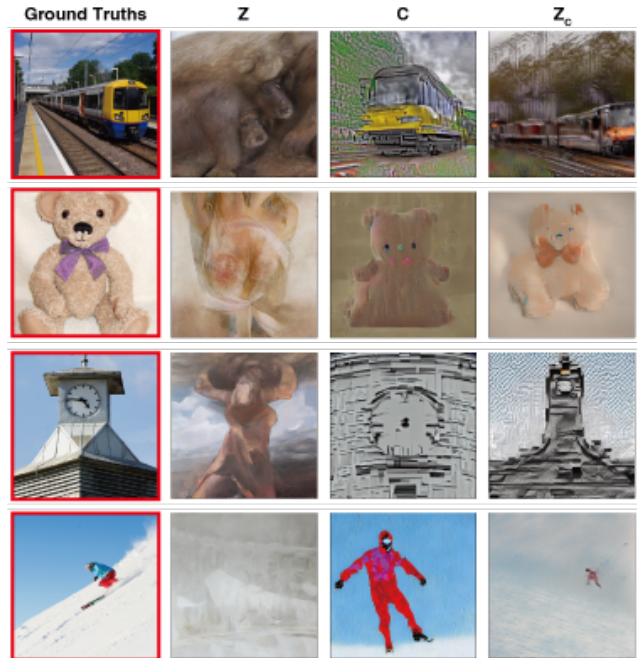

Figure 3. Presented (red box) and reconstructed images for a single subject (subj01) using $\mathbf{z}$, $\mathbf{c}$, and $\mathbf{z_c}$.

4. Results

4.1. Decoding

Figure 3 shows the results of visual reconstruction for one subject (subj01). We generated five images for each test image and selected the generated images with highest PSMs. On the one hand, images reconstructed using only $\mathbf{z}$ were visually consistent with the original images, but failed to capture their semantic content. On the other hand, images reconstructed using only $\mathbf{c}$ generated images with high semantic fidelity but were visually inconsistent. Finally, images reconstructed using $\mathbf{z_c}$ could generate high-resolution images with high semantic fidelity (see Appendix B for more examples).

Figure 4 shows reconstructed images from all subjects for the same image (all images were generated using $\mathbf{z_c}$. Other examples are available in the Appendix B). Overall, reconstruction quality was stable and accurate across subjects.

We note that, the lack of agreement regarding specific details of the reconstructed images may differences in perceived experience across subjects, rather than failures of reconstruction. Alternatively it may simply reflect differences in data quality among subjects. Indeed, subjects with high (subj01) and low (subj07) decoding accuracy from fMRI were subjects with high and low data quality metrics, respectively (see Appendix B).

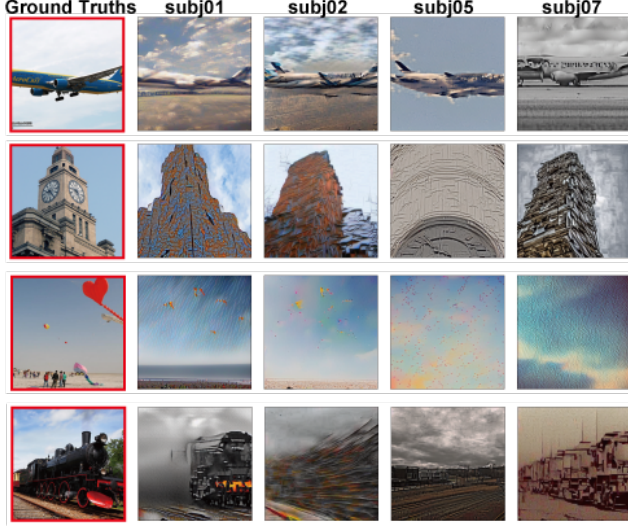Figure 5 plots results for the quantitative evaluation. In

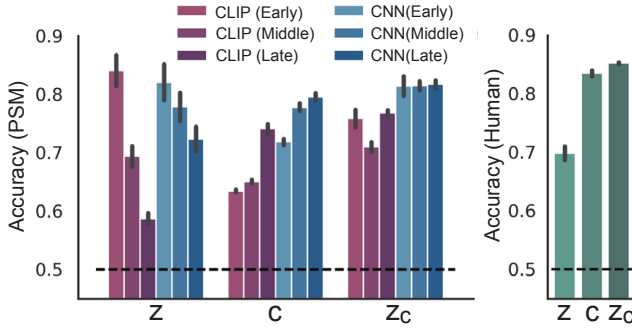Figure 4. Example results for all four subjects.

Figure 5. Identification accuracy calculated using objective (left) and subjective (right) criteria (pooled across four subjects; chance level corresponds to 50%). Error bars indicate standard error of the mean.

fewer images, much less image complexity (typically individual objects positioned in the center of the image), and lack full-text annotations of the kind available from NSD. Only one study to date [25] used NSD for visual reconstruction, and they reported accuracy values of $78 \pm 4.5\%$ for one subject (subj01) using PSM based on Inception V3. It is difficult to draw a direct comparison with this study, because it differed from ours in several respects (for example, it used different training and test sample sizes, and different image resolutions). Notwithstanding these differences, their reported values fall within a similar range to ours for the same subject (77% using CLIP, 83% using AlexNet, and 76% using Inception V3). However, this prior study relied on extensive model training and feature engineering with many more hyper-parameters than those adopted in our study, including the necessity to train complex generative models, fine-tuning toward MS COCO, data augmentation, and arbitrary thresholding of features. We did not use any of the above techniques — rather, our simple pipeline only requires the construction of two linear regression models from fMRI activity to latent representations of LDM.

Furthermore, we observed a reduction in semantic fidelity when we used categorical information associated with the images, rather than full-text annotations for **c**. We also found an increase in semantic fidelity when we used semantic maps instead of original images for **z**, though visual similarity was decreased in this case (see Appendix B).

4.2. Encoding Model

4.2.1 Comparison among Latent Representations

Figure 6 shows prediction accuracy of the encoding models for three types of latent representations associated with the LDM: **z**, a latent representation of the original image; **c**, a latent representation of image text annotation; and $\mathbf{z_c}$, a noise-added latent representation of **z** after reverse diffusion process with cross-attention to **c**.

Although all three components produced high prediction performance at the back of the brain, visual cortex, they showed stark contrast. Specifically, **z** produced high prediction performance in the posterior part of visual cortex, namely early visual cortex. It also showed significant prediction values in the anterior part of visual cortex, namely higher visual cortex, but smaller values in other regions. On the other hand, **c** produced the highest prediction performance in higher visual cortex. The model also showed high prediction performance across a wide span of cortex. $\mathbf{z_c}$ carries a representation that is very similar to **z**, showing high prediction performance for early visual cortex. Although this is somewhat predictable given their intrinsic similarity, it is nevertheless intriguing because these representations correspond to visually different generated images. We also observed that using $\mathbf{z_c}$ with a reduced noise level injected into **z** produces a more similar prediction map to the predic-

the objective evaluation, images reconstructed using $\mathbf{z_c}$ are generally associated with higher accuracy values across different metrics than images reconstructed using only **z** or **c**. When only **z** was used, accuracy values were particularly high for PSMs derived from early layers of CLIP and CNN. On the other hand, when only **c** was used, accuracy values were higher for PSMs derived from late layers. In the subjective evaluation, accuracy values of images obtained from **c** are higher than those obtained from **z**, while $\mathbf{z_c}$ resulted in the highest accuracy compared with the other two methods ($P < 0.01$ for all comparisons, two-sided signed-rank test, FWE corrected). Together, these results suggest that our method captures not only low-level visual appearance, but also high-level semantic content of the original stimuli.

It is difficult to compare our results with those reported by most previous studies, because they used different datasets. The datasets used in previous studies contain far
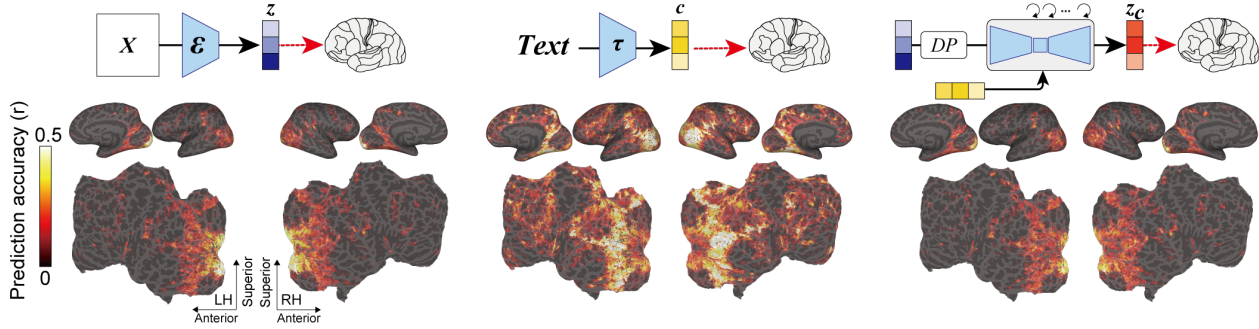
Figure 6. Prediction performance (measured using Pearson's correlation coefficients) for the voxel-wise encoding model applied to held-out test images in a single subject (subj01), projected onto the inflated (top, lateral and medial views) and flattened cortical surface (bottom, occipital areas are at the center), for both left and right hemispheres. Brain regions with significant accuracy are colored (all colored voxels $P < 0.05$, FDR corrected).

tion map obtained from $\mathbf{z}$, as expected (see Appendix C). This similarity prompted us to conduct an additional analysis to compare the unique variance explained by these two models, detailed in the following section. See Appendix C for results of all subjects.

4.2.2 Comparison across different noise levels

While the previous results showed that prediction accuracy maps for $\mathbf{z}$ and $\mathbf{z_c}$ present similar profiles, they do not tell us how much unique variance is explained by each feature as a function of different noise levels. To enhance our understanding of the above issues, we next constructed encoding models that simultaneously incorporated both $\mathbf{z}$ and $\mathbf{z_c}$ into a single model, and studied the unique contribution of each feature. We also varied the level of noise added to $\mathbf{z}$ for generating $\mathbf{z_c}$.

Figure 7 shows that, when a small amount of noise was added, $\mathbf{z}$ predicted voxel activity better than $\mathbf{z_c}$ across cortex. Interestingly, when we increased the level of noise, $\mathbf{z_c}$ predicted voxel activity within higher visual cortex better than $\mathbf{z}$, indicating that the semantic content of the image was gradually emphasized.

This result is intriguing because, without analyses like this, we can only observe randomly generated images, and we cannot examine how the text-conditioned image-to-image process is able to balance between semantic content and original visual appearance.

4.2.3 Comparison across different diffusion stages

We next asked how the noise-added latent representation changes over the iterative denoising process.

Figure 8 shows that, during the early stages of the denoising process, $\mathbf{z}$ signals dominated prediction of fMRI signals. During the middle step of the denoising process, $\mathbf{z_c}$ predicted activity within higher visual cortex much bet-
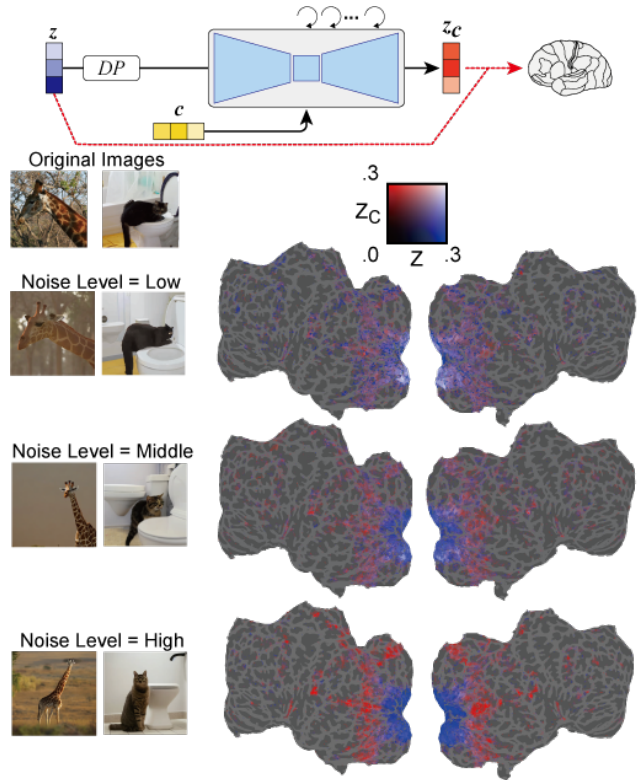

Figure 7. Unique variance accounted for by $\mathbf{z_c}$ compared with $\mathbf{z}$ in one subject (subj01), obtained by splitting accuracy values from the combined model. While fixing $\mathbf{z}$, we used $\mathbf{z_c}$ with varying amounts of noise-level added to the latent representation of stimuli from low-level (top) to high-level (bottom). All colored voxels $P < 0.05$, FDR corrected.

ter than $\mathbf{z}$, indicating that the bulk of the semantic content emerges at this stage. These results show how LDM refines and generates images from noise.
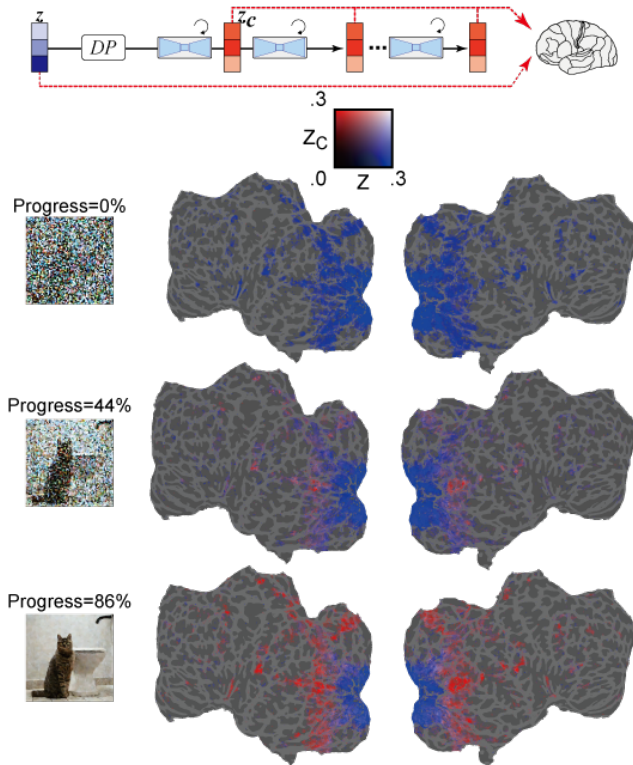
Figure 8. Unique variance accounted for by $\mathbf{z_c}$ compared with $\mathbf{z}$ in one subject (subj01), obtained by splitting accuracy values from the combined model. While fixing $\mathbf{z}$, we used $\mathbf{z_c}$ with different denoising stages from early (top) to late (bottom) steps. All colored voxels $P < 0.05$, FDR corrected.
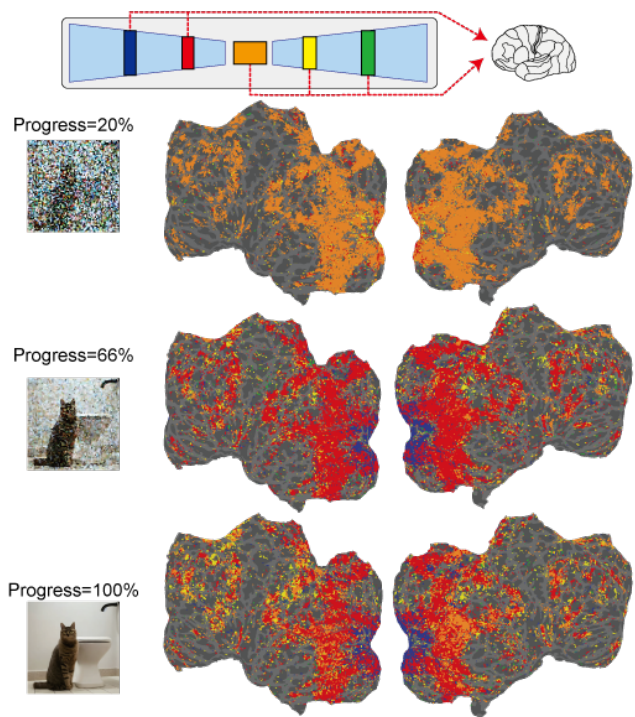

Figure 9. Selective engagement of different U-Net layers for different voxels across the brain. Colors represent the most predictive U-Net layer for early (top) to late (bottom) denoising steps. All colored voxels $P < 0.05$, FDR corrected.

4.2.4 Comparison across different U-Net Layers

Finally, we asked what information is being processed at each layer of U-Net.

Figure 9 shows the results of encoding models for different steps of the denoising process (early, middle, late), and for the different layers of U-Net. During the early phase of the denoising process, the bottleneck layer of U-Net (colored orange) produces the highest prediction performance across cortex. However, as denoising progresses, the early layer of U-Net (colored blue) predicts activity within early visual cortex, and the bottleneck layer shifts toward superior predictive power for higher visual cortex.

These results suggest that, at the beginning of the reverse diffusion process, image information is compressed within the bottleneck layer. As denoising progresses, a functional dissociation among U-Net layers emerges within visual cortex: i.e., the first layer tends to represent fine-scale details in early visual areas, while the bottleneck layer corresponds to higher-order information in more ventral, semantic areas.

5. Conclusions

We propose a novel visual reconstruction method using LDMs. We show that our method can reconstruct high-resolution images with high semantic fidelity from human brain activity. Unlike previous studies of image reconstruction, our method does not require training or fine-tuning of complex deep-learning models: it only requires simple linear mappings from fMRI to latent representations within LDMs.

We also provide a quantitative interpretation for the internal components of the LDM by building encoding models. For example, we demonstrate the emergence of semantic content throughout the inverse diffusion process, we perform layer-wise characterization of U-Net, and we provide a quantitative interpretation of image-to-image transformations with different noise levels. Although DMs are developing rapidly, their internal processes remain poorly understood. This study is the first to provide a quantitative interpretation from a biological perspective.

References

[1] Emily J. Allen, Ghislain St-Yves, Yihan Wu, Jesse L. Breedlove, Jacob S. Prince, Logan T. Dowdle, Matthias Nau, Brad Caron, Franco Pestilli, Ian Charest, J. Benjamin Hutchinson, Thomas Naselaris, and Kendrick Kay. A massive 7t fmri dataset to bridge cognitive neuroscience and artificial intelligence. *Nature Neuroscience*, 25:116–126, 1 2022. 3

[2] Roman Beliy, Guy Gaziv, Assaf Hoogi, Francesca Strappini, Tal Golan, and Michal Irani. From voxels to pixels and back: Self-supervision in natural-image reconstruction from fmri. *Advances in Neural Information Processing Systems*, 32, 2019. 2

[3] Charlotte Caucheteux and Jean-Rémi King. Brains and algorithms partially converge in natural language processing. *Communications biology*, 5(1):1–10, 2022. 1, 3

[4] Prafulla Dhariwal and Alexander Nichol. Diffusion models beat gans on image synthesis. *Advances in Neural Information Processing Systems*, 34:8780–8794, 2021. 2

[5] Tao Fang, Yu Qi, and Gang Pan. Reconstructing perceptive images from brain activity by shape-semantic gan. *Advances in Neural Information Processing Systems*, 33:13038–13048, 2020. 2

[6] Jin Gao, Jialing Zhang, Xihui Liu, Trevor Darrell, Evan Shelhamer, and Dequan Wang. Back to the source: Diffusion-driven test-time adaptation. *arXiv preprint arXiv:2207.03442*, 2022. 2

[7] Guy Gaziv, Roman Beliy, Niv Granot, Assaf Hoogi, Francesca Strappini, Tal Golan, and Michal Irani. Self-supervised natural image reconstruction and large-scale semantic classification from brain activity. *NeuroImage*, 254, 7 2022. 2

[8] Ariel Goldstein, Zaid Zada, Eliav Buchnik, Mariano Schain, Amy Price, Bobbi Aubrey, Samuel A Nastase, Amir Feder, Dotan Emanuel, Alon Cohen, et al. Shared computational principles for language processing in humans and deep language models. *Nature neuroscience*, 25(3):369–380, 2022. 1, 3

[9] Iris IA Groen, Michelle R Greene, Christopher Baldassano, Li Fei-Fei, Diane M Beck, and Chris I Baker. Distinct contributions of functional and deep neural network features to representational similarity of scenes in human brain and behavior. *Elife*, 7, 2018. 1, 3

[10] Umut Güçlü and Marcel AJ van Gerven. Deep neural networks reveal a gradient in the complexity of neural representations across the ventral stream. *Journal of Neuroscience*, 35(27):10005–10014, 2015. 1, 3

[11] Jonathan Ho, Ajay Jain, and Pieter Abbeel. Denoising diffusion probabilistic models. *Advances in Neural Information Processing Systems*, 33:6840–6851, 2020. 2, 4

[12] Tomoyasu Horikawa, Alan S Cowen, Dacher Keltner, and Yukiyasu Kamitani. The neural representation of visually evoked emotion is high-dimensional, categorical, and distributed across transmodal brain regions. *Iscience*, 23(5):101060, 2020. 2

[13] Tomoyasu Horikawa and Yukiyasu Kamitani. Generic decoding of seen and imagined objects using hierarchical vi-

sual features. *Nature communications*, 8(1):1–15, 2017. 1, 2, 3

[14] Tomoyasu Horikawa, Masako Tamaki, Yoichi Miyawaki, and Yukiyasu Kamitani. Neural decoding of visual imagery during sleep. *Science*, 340(6132):639–642, 2013. 2

[15] Alexander G Huth, Tyler Lee, Shinji Nishimoto, Natalia Y Bilenko, An T Vu, and Jack L Gallant. Decoding the semantic content of natural movies from human brain activity. *Frontiers in systems neuroscience*, 10:81, 2016. 2

[16] Bahjat Kawar, Jiaming Song, Stefano Ermon, and Michael Elad. Jpeg artifact correction using denoising diffusion restoration models. *arXiv preprint arXiv:2209.11888*, 2022. 2

[17] Kendrick N Kay, Thomas Naselaris, Ryan J Prenger, and Jack L Gallant. Identifying natural images from human brain activity. *Nature*, 452(7185):352–355, 2008. 2

[18] Alexander JE Kell, Daniel LK Yamins, Erica N Shook, Sam V Norman-Haignere, and Josh H McDermott. A task-optimized neural network replicates human auditory behavior, predicts brain responses, and reveals a cortical processing hierarchy. *Neuron*, 98(3):630–644, 2018. 1, 3

[19] Tim C Kietzmann, Courtney J Spoerer, Lynn KA Sörensen, Radoslaw M Cichy, Olaf Hauk, and Nikolaus Kriegeskorte. Recurrence is required to capture the representational dynamics of the human visual system. *Proceedings of the National Academy of Sciences*, 116(43):21854–21863, 2019. 1, 3

[20] Naoko Koide-Majima, Tomoya Nakai, and Shinji Nishimoto. Distinct dimensions of emotion in the human brain and their representation on the cortical surface. *NeuroImage*, 222:117258, 2020. 2

[21] Takuya Koumura, Hiroki Terashima, and Shigeto Furukawa. Cascaded tuning to amplitude modulation for natural sound recognition. *Journal of Neuroscience*, 39(28):5517–5533, 2019. 1, 3

[22] Alex Krizhevsky, Ilya Sutskever, and Geoffrey E Hinton. Imagenet classification with deep convolutional neural networks. *Communications of the ACM*, 60(6):84–90, 2017. 4, 13

[23] T. D. la Tour, M. Eickenberg, A. O. Nunez-Elizalde, and J. L. Gallant. Feature-space selection with banded ridge regression. *NeuroImage*, page 119728, Nov 2022. 5

[24] Lynn Le, Luca Ambrogioni, Katja Seeliger, Yağmur Güçlütürk, Marcel van Gerven, and Umut Güçlü. Brain2pix: Fully convolutional naturalistic video reconstruction from brain activity. *BioRxiv*, 2021. 2

[25] Sikun Lin, Thomas Sprague, and Ambuj K Singh. Mind reader: Reconstructing complex images from brain activities. *Advances in Neural Information Processing Systems*, 9 2022. 2, 6

[26] Yoichi Miyawaki, Hajime Uchida, Okito Yamashita, Masaaki Sato, Yusuke Morito, Hiroki C. Tanabe, Norihiro Sadato, and Yukiyasu Kamitani. Visual image reconstruction from human brain activity using a combination of multiscale local image decoders. *Neuron*, 60:915–929, 12 2008. 2

[27] Milad Mozafari, Leila Reddy, and Rufin VanRullen. Reconstructing natural scenes from fMRI patterns using bigbigan.

In *2020 International joint conference on neural networks (IJCNN)*, pages 1–8. IEEE, 2020. 2

[28] Tomoya Nakai and Shinji Nishimoto. Quantitative models reveal the organization of diverse cognitive functions in the brain. *Nature communications*, 11(1):1–12, 2020. 2

[29] Thomas Naselaris, Cheryl A Olman, Dustin E Stansbury, Kamil Ugurbil, and Jack L Gallant. A voxel-wise encoding model for early visual areas decodes mental images of remembered scenes. *Neuroimage*, 105:215–228, 2015. 2

[30] Thomas Naselaris, Ryan J Prenger, Kendrick N Kay, Michael Oliver, and Jack L Gallant. Bayesian reconstruction of natural images from human brain activity. *Neuron*, 63(6):902–915, 2009. 2

[31] Satoshi Nishida and Shinji Nishimoto. Decoding naturalistic experiences from human brain activity via distributed representations of words. *Neuroimage*, 180:232–242, 2018. 2

[32] Shinji Nishimoto, An T. Vu, Thomas Naselaris, Yuval Benjamini, Bin Yu, and Jack L. Gallant. Reconstructing visual experiences from brain activity evoked by natural movies. *Current Biology*, 21:1641–1646, 10 2011. 2

[33] Vadim Popov, Ivan Vovk, Vladimir Gogoryan, Tasnima Sadekova, and Mikhail Kudinov. Grad-tts: A diffusion probabilistic model for text-to-speech. In *International Conference on Machine Learning*, pages 8599–8608. PMLR, 2021. 2

[34] Alec Radford, Jong Wook Kim, Chris Hallacy, Aditya Ramesh, Gabriel Goh, Sandhini Agarwal, Girish Sastry, Amanda Askell, Pamela Mishkin, Jack Clark, et al. Learning transferable visual models from natural language supervision. In *International Conference on Machine Learning*, pages 8748–8763. PMLR, 2021. 4

[35] Zarina Rakhimberdina, Quentin Jodelet, Xin Liu, and Tsuyoshi Murata. Natural image reconstruction from fmri using deep learning: A survey. *Frontiers in Neuroscience*, 15, 2021. 13

[36] Ziqi Ren, Jie Li, Xuetong Xue, Xin Li, Fan Yang, Zhicheng Jiao, and Xinbo Gao. Reconstructing seen image from brain activity by visually-guided cognitive representation and adversarial learning. *NeuroImage*, 228:117602, 2021. 2

[37] Robin Rombach, Andreas Blattmann, Dominik Lorenz, Patrick Esser, and Björn Ommer. High-resolution image synthesis with latent diffusion models. In *Proceedings of the IEEE/CVF Conference on Computer Vision and Pattern Recognition*, pages 10684–10695, 2022. 2

[38] Chitwan Saharia, William Chan, Huiwen Chang, Chris Lee, Jonathan Ho, Tim Salimans, David Fleet, and Mohammad Norouzi. Palette: Image-to-image diffusion models. In *ACM SIGGRAPH 2022 Conference Proceedings*, pages 1–10, 2022. 2

[39] Chitwan Saharia, William Chan, Saurabh Saxena, Lala Li, Jay Whang, Emily Denton, Seyed Kamyar Seyed Ghasemipour, Burcu Karagol Ayan, S Sara Mahdavi, Rapha Gontijo Lopes, et al. Photorealistic text-to-image diffusion models with deep language understanding. *Advances in Neural Information Processing Systems*, 2022. 2

[40] Chitwan Saharia, Jonathan Ho, William Chan, Tim Salimans, David J Fleet, and Mohammad Norouzi. Image super-resolution via iterative refinement. *IEEE Transactions on Pattern Analysis and Machine Intelligence*, 2022. 2

[41] Hiroshi Sasaki, Chris G Willcocks, and Toby P Breckon. Unit-ddpm: Unpaired image translation with denoising diffusion probabilistic models. *arXiv preprint arXiv:2104.05358*, 2021. 2

[42] Lea-Maria Schmitt, Julia Erb, Sarah Tune, Anna U Rysop, Gesa Hartwigsen, and Jonas Obleser. Predicting speech from a cortical hierarchy of event-based time scales. *Science Advances*, 7(49):eabi6070, 2021. 1, 3

[43] Martin Schrimpf, Idan Asher Blank, Greta Tuckute, Carina Kauf, Eghbal A Hosseini, Nancy Kanwisher, Joshua B Tenenbaum, and Evelina Fedorenko. The neural architecture of language: Integrative modeling converges on predictive processing. *Proceedings of the National Academy of Sciences*, 118(45):e2105646118, 2021. 1, 3

[44] Katja Seeliger, Umut Güçlü, Luca Ambrogioni, Yagmur Güçlütürk, and Marcel AJ van Gerven. Generative adversarial networks for reconstructing natural images from brain activity. *NeuroImage*, 181:775–785, 2018. 2

[45] Guohua Shen, Kshitij Dwivedi, Kei Majima, Tomoyasu Horikawa, and Yukiyasu Kamitani. End-to-end deep image reconstruction from human brain activity. *Frontiers in Computational Neuroscience*, page 21, 2019. 2

[46] Guohua Shen, Tomoyasu Horikawa, Kei Majima, and Yukiyasu Kamitani. Deep image reconstruction from human brain activity. *PLoS Computational Biology*, 15, 2019. 2

[47] Jascha Sohl-Dickstein, Eric Weiss, Niru Maheswaranathan, and Surya Ganguli. Deep unsupervised learning using nonequilibrium thermodynamics. In *International Conference on Machine Learning*, pages 2256–2265. PMLR, 2015. 2, 4

[48] Yang Song and Stefano Ermon. Generative modeling by estimating gradients of the data distribution. *Advances in Neural Information Processing Systems*, 32, 2019. 2

[49] Yang Song, Jascha Sohl-Dickstein, Diederik P Kingma, Abhishek Kumar, Stefano Ermon, and Ben Poole. Score-based generative modeling through stochastic differential equations. *International Conference on Learning Representations*, 2020. 2

[50] Christian Szegedy, Vincent Vanhoucke, Sergey Ioffe, Jon Shlens, and Zbigniew Wojna. Rethinking the inception architecture for computer vision. In *Proceedings of the IEEE conference on computer vision and pattern recognition*, pages 2818–2826, 2016. 13

[51] Yu Takagi, Yuki Sakai, Yoshinari Abe, Seiji Nishida, Ben J Harrison, Ignacio Martínez-Zalacaín, Carles Soriano-Mas, Jin Narumoto, and Saori C Tanaka. A common brain network among state, trait, and pathological anxiety from whole-brain functional connectivity. *Neuroimage*, 172:506–516, 2018. 2

[52] Jerry Tang, Amanda LeBel, Shailee Jain, and Alexander G Huth. Semantic reconstruction of continuous language from non-invasive brain recordings. *bioRxiv*, 2022. 2

[53] Pascal Vincent. A connection between score matching and denoising autoencoders. *Neural computation*, 23(7):1661–1674, 2011. 2

[54] Haiguang Wen, Junxing Shi, Yizhen Zhang, Kun-Han Lu, Ji-ayue Cao, and Zhongming Liu. Neural encoding and decoding with deep learning for dynamic natural vision. *Cerebral cortex*, 28(12):4136–4160, 2018. 1, 3

[55] Daniel LK Yamins, Ha Hong, Charles F Cadieu, Ethan A Solomon, Darren Seibert, and James J DiCarlo. Performance-optimized hierarchical models predict neural responses in higher visual cortex. *Proceedings of the national academy of sciences*, 111(23):8619–8624, 2014. 1, 3